Biofilm carrier migration model describes reactor performance

Joshua P. Boltz, Bruce R. Johnson, Imre Takács, Glen T. Daigger, Eberhard Morgenroth, Doris Brockmann, Róbert Kovács, Jason M. Calhoun, Jean-Marc Choubert and Nicolas Derlon

ABSTRACT

The accuracy of a biofilm reactor model depends on the extent to which physical system conditions (particularly bulk-liquid hydrodynamics and their influence on biofilm dynamics) deviate from the ideal conditions upon which the model is based. It follows that an improved capacity to model a biofilm reactor does not necessarily rely on an improved biofilm model, but does rely on an improved mathematical description of the biofilm reactor and its components. Existing biofilm reactor models typically include a one-dimensional biofilm model, a process (biokinetic and stoichiometric) model, and a continuous flow stirred tank reactor (CFSTR) mass balance that [when organizing CFSTRs in series] creates a pseudo two-dimensional (2-D) model of bulk-liquid hydrodynamics approaching plug flow. In such a biofilm reactor model, the user-defined biofilm area is specified for each CFSTR; thereby, $X_{carrier}$ does not exit the boundaries of the CFSTR to which they are assigned or exchange boundaries with other CFSTRs in the series. The error introduced by this pseudo 2-D biofilm reactor modeling approach may adversely affect model results and limit model-user capacity to accurately calibrate a model. This paper presents a new sub-model that describes the migration of $X_{carrier}$ and associated biofilms, and evaluates the impact that $X_{carrier}$ migration and axial dispersion has on simulated system performance. Relevance of the new biofilm reactor model to engineering situations is discussed by applying it to known biofilm reactor types and operational conditions.

Key words | biofilm, design, model, reactor, wastewater

Joshua P. Boltz (corresponding author)
Volkert,
3809 Moffett Rd,
Mobile, AL 36618, USA
E-mail: *jboltz@volkert.com*

Bruce R. Johnson
CH2M,
9191 S. Jamaica St.,
Englewood, CO 80112, USA

Imre Takács
Róbert Kovács
Dynamita,
7 Eoupe, La Redoute,
Nyons 26110, France

Glen T. Daigger
University of Michigan,
1351 Beal Avenue, 177 EWRE,
Ann Arbor, MI 48109, USA

Eberhard Morgenroth
Nicolas Derlon
ETH Zürich,
Institute of Environmental Engineering,
Zürich 8093, Switzerland
and
EAWAG,
Swiss Federal Institute of Aquatic Science and Technology,
Dübendorf 8600, Switzerland

Doris Brockmann
INRA Transfert Environnement,
Avenue des Etangs,
Narbonne F-11100, France

Jason M. Calhoun
Renewable Fibers Wastewater (RF WW),
733 W. Johnson St., Ste. 200,
Raleigh, NC 27603, USA

Jean-Marc Choubert
IRSTEA, UR MALY,
5 rue de la Doua BP 32108,
Villeurbanne, FR 69616, France

INTRODUCTION

One-dimensional (1-D) biofilm models are accurate for simulating biofilm reactors (Morgenroth *et al.* 2000). Boltz *et al.* (2010) evaluated and summarized biofilm (reactor) models in existing wastewater treatment plant (WWTP) simulators. Typically, existing biofilm reactor models include a 1-D biofilm model, a biokinetic model, and a continuous flow stirred tank reactor (CFSTR) module that (when organized in series) creates a pseudo two-dimensional (2-D) model of bulk-liquid hydrodynamics approaching plug flow. In such an existing biofilm reactor

doi: 10.2166/wst.2017.160

model, a user-defined biofilm area (A_F) is specified for each CFSTR, which is akin to the retention/isolation of free-moving submerged biofilm carriers ($X_{carrier}$) in any CFSTR (i.e., $X_{carrier}$ does not exit the boundaries of the CFSTR to which they are assigned, or exchange boundaries with other CFSTRs in the series). Rittmann (1982) defined a well operating biofilm reactor with $X_{carrier}$ as having a hydrodynamic regime approaching plug flow while the $X_{carrier}$ population and associated biofilms are completely mixed despite L:W≫1 (i.e., the biofilm biomass distribution is equal throughout the reactor).

The accuracy of existing biofilm reactor models is largely defined by the extent to which physical system conditions – particularly, bulk-liquid hydrodynamics and biofilm dynamics – deviate from the ideal conditions upon which the model is based (Boltz & Daigger 2010). Boltz *et al.* (2011) systematically evaluated the ability of existing biofilm models to describe systems having $X_{carrier}$ while using a common modeling platform (i.e., AQUASIM), and assessed the identifiability of key model parameters. Boltz *et al.* (2012) outlined a Good Biofilm Reactor Modeling Practice (GBRMP). A component of GBRMP is the calibration protocol. Brockmann *et al.* (2013) reported evidence of modeling limitations when the GBRMP was applied to a nitrifying moving bed biofilm reactor (MBBR) that deviates from ideal completely mixed bulk-liquid hydrodynamics. An improved capacity to model a biofilm reactor does not necessarily rely on an improved biofilm model, but does rely on an improved mathematical description of the biofilm reactor and its components. This notion is particularly relevant when considering that biofilm reactors containing $X_{carrier}$ are presently the most widely applied biofilm-based system(s) for municipal and industrial wastewater treatment.

Existing biofilm reactor models, which require a user-defined A_F in each CFSTR, simulate biofilm biomass distribution (in 1-D perpendicular to the growth medium) as a function of substrate availability and environmental conditions in each respective CFSTR. Isolating portions of an $X_{carrier}$ population and associated biofilms in different CFSTRs results in different simulated biofilm biomass compositions in each CFSTR, which can impact the simulated value of flux of any substrate i ($J_{F,i}$). This results in the number of different biofilm biomass compositions and $J_{F,i}$ values for any simulated biofilm reactor being defined by the number of CFSTRs in series. The error introduced by this pseudo 2-D biofilm reactor modeling approach may adversely affect model results and limit a model user's capacity to accurately calibrate the model. This paper presents and evaluates a biofilm reactor sub-model that accounts for the movement of an $X_{carrier}$ population and associated biofilms through any number of CFSTRs in series, affiliated connection/recirculation stream(s), and the biofilm reactor coupled liquid-solid separation unit process. The objective of our investigation is to ascertain the sub-model's capacity for describing biofilm reactor performance when $X_{carrier}$ is present.

MATERIALS AND METHODS

Formulating a larger, more widely functional model using a combination of focused models, or sub-models, to describe a unit process is commonly employed when modeling municipal and industrial wastewater treatment processes. Biofilm reactor models typically include the following sub-models: (1) process, kinetic, and stoichiometric model (e.g., ASM3 and ASM2d); (2) pseudo-analytical, analytical, or numerical 1-D biofilm model; and (3) bulk-liquid hydrodynamic model. A biofilm reactor model also typically includes user-defined streams that account for internal recirculation, biomass wasting, and constituent introduction from external tanks (e.g., nutrients or flows from other unit processes).

This paper presents a sub-model that simulates $X_{carrier}$ population and associated biofilms' heterogeneity throughout a biofilm reactor. Accurate implementation of this sub-model depends on the model user understanding the difference between $X_{carrier}$ (and associated biofilm) *movement* and *migration*. Biofilm reactors with $X_{carrier}$ *movement* is defined here as mixing conditions that result in the even distribution of an $X_{carrier}$ population and associated biofilms, throughout, whereby the A_F is uniformly exposed to substrates in the bulk liquid of a CFSTR. *Migration* is defined here as an $X_{carrier}$ population and associated biofilms flowing through any number of CFSTRs in series and affiliated connection/recirculation stream(s) used to simulate a biofilm reactor (and coupled liquid-solid separation unit process, if applicable). Migration of $X_{carrier}$ results in the A_F being uniformly exposed to substrates in the bulk-liquid of each CFSTR through which $X_{carrier}$ passes during the simulation specific, user-defined $X_{carrier}$ residence time in each respective CFSTR.

To further evaluate the migration of an $X_{carrier}$ population and associated biofilms, the reader should consider a rectangular (plan view) biofilm reactor having L:W ≫1, and a hydrodynamic condition that approaches ideal plug flow. The biofilm reactor is coupled with a liquid-solids separation unit process (e.g., sedimentation basin). By definition, $X_{carrier}$ can be retained in a specific bioreactor

zone, move throughout the entire biofilm reactor, or move throughout the entire biofilm reactor and its coupled liquid-solids separation unit process. If retained in the biofilm reactor (or a specific zone of the biofilm reactor), the tank is equipped with an $X_{carrier}$ retention construct (e.g., screens in an MBBR) or relies on gravity acting against the $X_{carrier}$ in an upward flowing liquid field (e.g., fluidized bed biofilm reactor or granule reactors). Kagawa *et al.* (2016) presented an aerobic granule reactor model that accounts for a mechanistic mathematical description of the biofilm coupled with a sequencing batch reactor model to evaluate both micro- and macro-scale system observations. An $X_{carrier}$ population and associated biofilms can be classified as one of the following four conditions or as a transient state:

1. *Configuration A*: The biofilm reactor (or zone thereof) plan L:W ≤ 1, $X_{carrier}$ is retained in the biofilm reactor, and – provided sufficient mixing energy – $X_{carrier}$ is *evenly* distributed throughout the biofilm reactor (or zone thereof). The hydrodynamic regime and $X_{carrier}$ population is completely mixed.
2. *Configuration B*: The biofilm reactor (or zone thereof) plan L:W $\gg 1$, $X_{carrier}$ is retained in the biofilm reactor (or zone thereof), and $X_{carrier}$ is *evenly* distributed throughout the biofilm reactor (or zone thereof) (i.e., $X_{carrier,\ inlet} = X_{carrier,\ effluent}$). The hydrodynamic regime is plug flow.
3. *Configuration C*: The biofilm reactor (or zone thereof) plan L:W $\gg 1$, $X_{carrier}$ is retained in the biofilm reactor (or zone thereof), and $X_{carrier}$ is *unevenly* distributed throughout the biofilm reactor (or zone thereof) (i.e., $X_{carrier,\ inlet} \neq X_{carrier,\ effluent}$). Hydrodynamic regime is plug flow with a large extent of axial dispersion.
4. *Configuration D*: The biofilm reactor (or zone thereof) plan L:W $\gg 1$, $X_{carrier}$ is not retained in the biofilm reactor (or zone thereof), and $X_{carrier}$ is *evenly* distributed throughout the biofilm reactor (or zone thereof). The hydrodynamic regime is plug flow. $X_{carrier}$ migrates throughout the secondary process (i.e., bioreactor and liquid-solids separation unit process), and $X_{carrier}$ egress is either with clarified effluent due to non-ideal liquid-solid separation, or with wasted biomass.

Sufficient $X_{carrier}$ migration towards the retention construct, or point of egress, results in $X_{carrier}$ accumulation in this location. *Configuration A* may be accurately simulated with existing biofilm reactor models, but is applied in this study to compare results from existing biofilm reactor models with results from an expanded biofilm reactor model that accounts for $X_{carrier}$ migration. *Configurations B* and *C* facilitate an evaluation of simulation results when $X_{carrier}$ migration is constrained inside the [physical] biofilm reactor (i.e., $X_{carrier}$ moves amongst CFSTRs, but does not enter the liquid-solids separation unit process). *Configuration D* is simulated as a Modified Ludzack Ettinger (MLE) process, and facilitates an evaluation of the impact that unimpeded $X_{carrier}$ migration throughout the bioreactor and liquid-solids separation unit process has on simulated system performance. A return activated sludge (RAS) stream is applied for $X_{carrier}$ accumulation since $X_{carrier}$ is not retained in the bioreactor. Solid-state variables (i.e., $X_{carrier}$ and suspended growth) have the same residence time if (1) a modeling device is not included to separate suspended growth from $X_{carrier}$ and (2) the rate of $X_{carrier}$ and suspended growth attrition (either due to non-ideal liquid-solid separation or with wasted biomass) is equivalent.

A description of the $X_{carrier}$ migration model and related mathematical treatments is presented as supplemental information (available with the online version of this paper). Migration of an $X_{carrier}$ population and associated biofilms has been modeled by recirculating $X_{carrier}$ (along with the biofilm, bulk liquid, and all constituents suspended in the bulk of the liquid). The $X_{carrier}$ recirculation stream may originate from any CFSTR ($i = 1, 2, \ldots, n-1, n$) and be directed to any CFSTR in the series. Migration modeling introduces the solid-state variable $X_{carrier}$. Simulation of *Configuration B* allows $X_{carrier}$ to pass through a recirculation stream from CFSTR_$n = 3$ to CFSTR_$n = 1$. Simulation of *Configuration C* allows $X_{carrier}$ back mixing to describe axial dispersion and allow the model user to account for an uneven distribution of the $X_{carrier}$ population and associated biofilms along the bioreactor length. Simulation of *Configuration D* describes $X_{carrier}$ recirculation in the RAS stream, and no $X_{carrier}$ attrition (with wasted biomass or in the liquid-solid separation unit process effluent stream). The 1-D biofilm model is described by Wanner & Reichert (1996). ASM3 was applied when simulating *Configurations A, B,* and *C*; the model and parameter values described by Henze *et al.* (2000) were used unless defined herein. A modified ASM2d was the biological process model applied when simulating *Configuration D*; the model and parameter values described by Boltz *et al.* (2009) were used unless defined herein. The simulated 1-D biofilm was discretized as a series of 10 layers, plus a mass transfer boundary layer for modeling resistance to mass transfer external to the biofilm surface while linking the bulk liquid with the biofilm. The relevance of our proposed biofilm reactor model was evaluated by application to engineering scenarios and a comparison of model results. Dynamic simulations were

executed using SUMO (Dynamita, Nyons, France; Kovács *et al.* 2013) or Pro2D[2] (CH2M HILL, Colorado, USA). The WWTP simulator used allows for the configuration of elements (e.g., CFSTR module, flow connector) to establish a user-defined process configuration.

Model configurations

Process configurations (A–D) are presented and modeled to analyze the impact that $X_{carrier}$ migration, distribution, and axial dispersion have on simulated biofilm reactor performance. Process flow diagrams illustrating these configurations are presented as Figure 1. *Configuration A* is described by three CFSTRs in series with each retaining a user-defined (equivalent) portion of the $X_{carrier}$ population and associated biofilms ($X_{carrier}$ does not migrate). *Configuration B* is described by three CFSTRs in series with a single recirculation stream. The recirculation stream transports $X_{carrier}$ and associated biofilms, the bulk liquid, and any constituents suspended in the bulk liquid from the last CFSTR (n) to the influent of the first CFSTR ($n = 1$). When simulating *Configuration B* the $X_{carrier}$ population and associated biofilms are, by definition, evenly distributed throughout the series of three CFSTRs. There are no $X_{carrier}$ remaining in the effluent stream (i.e., $X_{carrier}|_{eff} = 0$). *Configuration C* is described by three CFSTRs in series. Each CFSTR in the series (except for $n = 1$) has a stream recirculating a portion of the $X_{carrier}$ population and associated biofilms, the bulk liquid, and any constituents suspended in the bulk phase to the CFSTR immediately upstream (i.e., $CFSTR|_{n-1} \xleftarrow{RCY} CFSTR|_{n}$) to account for plug flow with a large extent of axial dispersion (via back mixing). This configuration allows the model user to simulate an uneven $X_{carrier}$ distribution throughout the biofilm reactor. *Configuration D* is described by three CFSTRs in series followed by an ideal liquid-solids separation unit. $X_{carrier}$ migration throughout the CFSTRs and liquid solid-separation unit is modeled with $X_{carrier}$ constraint accounted for by ideal removal from the waste biomass

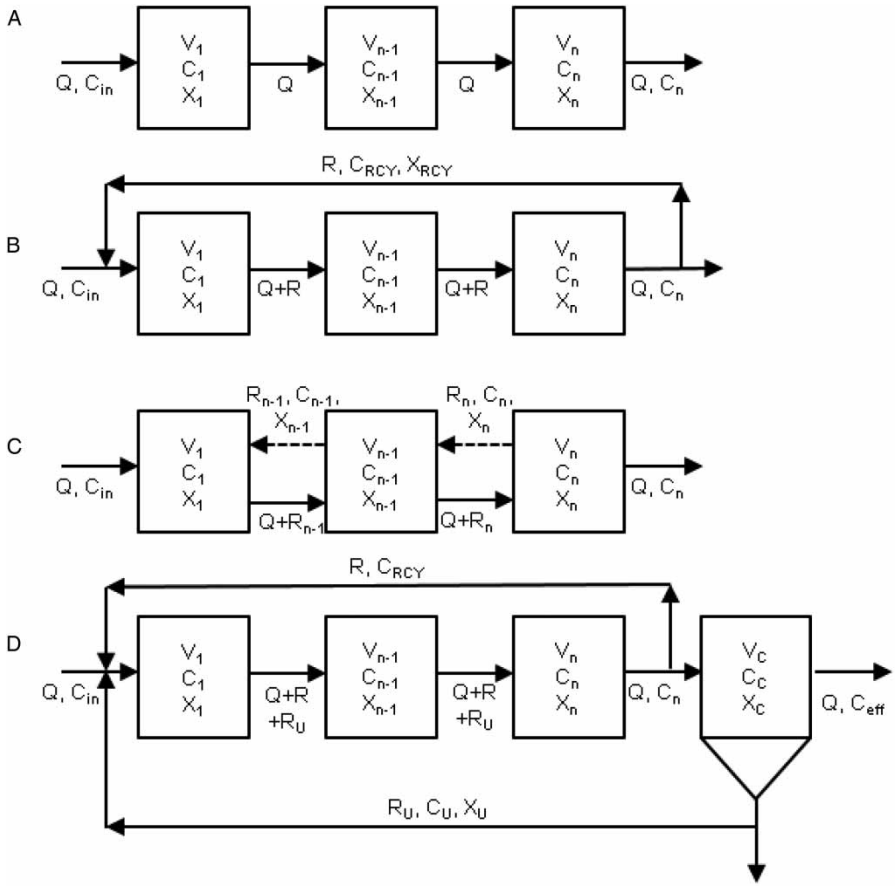

Figure 1 | Biofilm reactor hydrodynamic models: *Configuration A* with $X_{carrier}$ constrained in each CFSTR, *Configuration B* with $X_{carrier}$ migration through a series of n CFSTRs, *Configuration C* with $X_{carrier}$ migration and back-mixing, and *Configuration D* with $X_{carrier}$ migration throughout an MLE process and coupled liquid-solid separation unit.

and liquid-solid separation unit effluent stream. The $X_{carrier}$ population is recirculated with RAS.

Modeling the impact that $X_{carrier}$ location/migration has on biofilm reactor performance (quantified here as the simulated $J_{F,i}$) is approached differently with each process configuration. In *Configuration A*, $X_{carrier}$ is retained in each individual CFSTR; therefore, the A_F value in each CFSTR is input by the model user. In *Configuration B*, $X_{carrier}$ migrates and is uniformly distributed throughout the series of CFSTRs (i.e., the A_F value in each CFSTR is equal and is established by the $X_{carrier}$ specific surface area (A_S [=] m^2/m^3) defined by the model user). In *Configuration C*, $X_{carrier}$ migrates and accounts for uneven A_F distribution throughout the CFSTR series; therefore, the value of A_F in each CFSTR can be modified by the model user through manipulation of each back-mixing stream flow rate. In *Configuration D*, $X_{carrier}$ migrates throughout the CFSTR series and liquid-solid separation unit, which allows for $X_{carrier}$ and suspended biomass accumulation, $X_{carrier}$ is uniformly distributed throughout the series of CFSTRs (i.e., the value of A_F is equal in each CFSTR). Each of these modeling approaches requires a user-defined A_F or A_S, and recirculation stream flow rate (R) when appropriate.

Simulations: *Configurations A, B*, and *C*

Simulated *Configurations A*, *B*, and *C* consist of three CFSTRs in series designated MBBR_1, MBBR_2, and MBBR_3. The simulated processes are defined as a tertiary nitrifying biofilm reactor according to McQuarrie & Boltz (2011): BOD_5:TKN ≤ 1.0 and soluble $BOD_5 \leq 12$ g/m^3 (BOD_5: biochemical oxygen demand; TKN: total Kjeldahl nitrogen). The dissolved oxygen concentration (S_{F,O_2}) is rate-limiting inside the biofilm compartment of each simulated CFSTR. Simulated biofilm reactor influent wastewater constituent concentrations, physical characteristics of $X_{carrier}$, and biofilm model parameter values are listed as supplemental information. Each of the three CFSTRs has a 90 m^3 volume (V). The influent wastewater flow rate is (Q=) 3,785 m^3/d, and the bulk-liquid temperature was 17 °C for each simulation. *Configurations A* and *B* were modeled with (A_F=) 52,650 m^2 in each of the three CFSTRs. *Configuration B* was modeled with an $X_{carrier}$ recirculation rate set to 200% of the influent wastewater flow rate (i.e., $Q_{RCY} = 2 \times 3{,}785$ m^3/d = 7,570 m^3/d) which was adequate for $X_{carrier}$ to approach an ideal completely mixed condition. The total A_F of ($3 \times 52{,}650$ m^2=) 157,950 m^2 was evenly distributed throughout the biofilm reactor when simulating *Configurations A* and *B*. The individual recirculation streams surrounding each CFSTR were adjusted when modeling *Configuration C*. The recirculation stream flow rates were manipulated until the $X_{carrier}$ distribution resulted in A_F being 10-30-60 percentage of the total. The resulting A_F in each CFSTR ($n = 1$, 2, and 3) of *Configuration C* was 15,795 m^2, 47,385 m^2, and 94,770 m^2, respectively.

Simulations: *Configuration D*

A MLE process with a 250% internal mixed liquor recirculation flow rate including a suspended growth compartment, a biofilm compartment, or combined suspended growth and biofilm compartments (i.e., integrated fixed film activated sludge, IFAS) was simulated as *Configuration D*. The simulated process consists of three CFSTRs in series designated ANOXIC_1, AEROBIC_1, and AEROBIC_2. Physical characteristics of $X_{carrier}$ and biofilm model parameter values are listed as supplemental information. The influent wastewater flow rate was (Q=) 3,785 m^3/d, and the bulk-liquid temperature was 17 °C for each simulation. Total bioreactor volume was 1,420 and 473 m^3 for the suspended growth and IFAS/migrating $X_{carrier}$ simulations, respectively. The total A_F was 118,250-m^2, and was evenly distributed throughout CFSTRs in series. Suspended growth solids residence time was 9.1 and 2.3 days for the suspended growth and IFAS simulations, respectively. The mixed liquor total suspended solids concentration (X_{TSS}) was 2,350 and 2,280 g/m^3 for the suspended growth and IFAS simulations, respectively. Bulk-liquid dissolved oxygen concentration(s) were set to 4 g O_2/m^3 in aerobic zones. Dynamic simulations were executed using a diurnally varying influent that was equal on a day-to-day basis, and were run for 100 days. Normalized diurnal profiles for flow rate and pollutant loads were applied to average day values for steady-state simulations to quantify diurnal flow rate and pollutant load profiles. The assumed peak hydraulic load was 140% of the average day value ($1.4 \times 3{,}785 = 5{,}299$ m^3/day), and the assumed peak pollutant load was 170% of the average day value. The average day influent chemical oxygen demand (COD) concentration was 292 g/m^3, and the average influent ammonia-nitrogen concentration ($S_{B,A}$=) 30 g/m^3.

RESULTS AND DISCUSSION

Results of modeling *Configurations A* and *B* are presented in Figure 2. Simulated $J_{F,A}$ values obtained when $X_{carrier}$ is isolated in respective CFSTRs are compared with $J_{F,A}$ values obtained when modeling $X_{carrier}$ migration. Isolating $X_{carrier}$

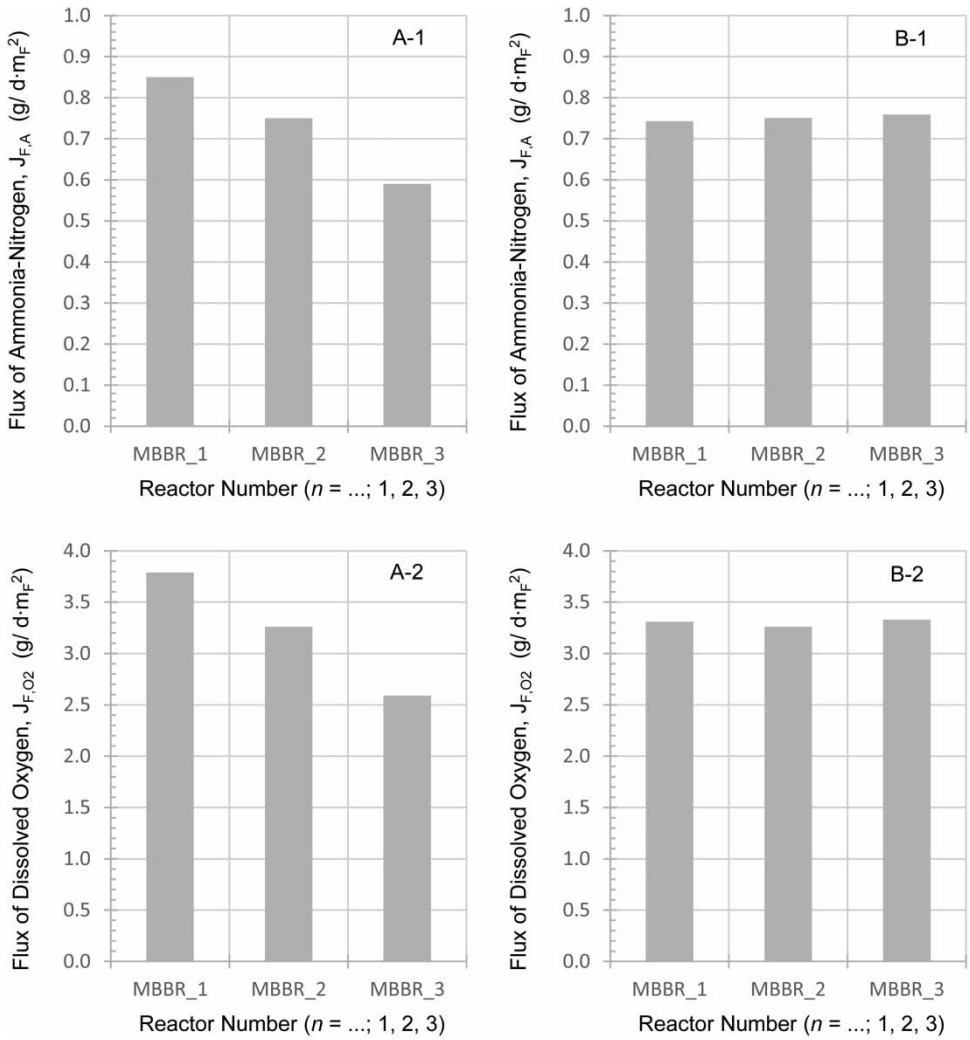

Figure 2 | Comparison of ammonia-nitrogen flux ($J_{F,A}$) [A-1, B-1], and dissolved oxygen flux (J_{F,O_2}) [A-2, B-2] when modeling *Configurations A* and *B*.

results in different $J_{F,A}$ values in each CFSTR: MBBR_1 $J_{F,A} = 0.85$ g/m^2/d; MBBR_2 $J_{F,A} = 0.75$ g/m^2/d; and MBBR_3 $J_{F,A} = 0.59$ g/m^2/d). Simulating $X_{carrier}$ migration resulted in a nearly equivalent $J_{F,A}$ value in each CFSTR: MBBR_1 – MBBR_3 $J_{F,A} = 0.74 \pm 0.01$ g/m^2/d). The simulation of *Configuration A* resulted in an $S_{B,A}$ conversion of 77.5%, and simulation of *Process Configuration B* resulted in an $S_{B,A}$ conversion of 78.0%.

Simulated dissolved oxygen flux (J_{F,O_2}) values also vary when $X_{carrier}$ is isolated in respective CFSTRs. Figure 2 illustrates nearly equivalent values of J_{F,O_2} obtained when simulating $X_{carrier}$ migration throughout *Configuration B*. Such model output can potentially offer significant implications for air diffuser grid design. An air-diffuser grid designed to accommodate *Configuration A* would require substantial tapering while the air-diffuser grid for *Configuration B* would be nearly uniform.

Another comparison facilitated by simulating *Configuration A* and *B* is the impact of modeling $X_{carrier}$ migration on the make-up and (1-D) distribution of biomass inside the biofilm. As presented in Figure 3 (A), the average autotrophic nitrifying organism concentration inside the biofilm ($X_{F,N}$) is greatest in MBBR_1 with subsequent ($X_{F,N}$) reduction in MBBR_2 and MBBR_3. Figure 3 (B) indicates that simulating $X_{carrier}$ migration results in a nearly equivalent (average) $X_{F,N}$ in each of the three CFSTRs. Simulations of *Configuration C* (which applies a 10-30-60 percentage distribution of A_F in MBBR_1, MBBR_2, and MBBR_3, respectively) were executed to evaluate the impact of variable $X_{carrier}$ distribution on $J_{F,A}$ and J_{F,O_2}. Figure 4 demonstrates that $J_{F,A}$ and J_{F,O_2} values are approximately equivalent in each of the CFSTRs. While these flux values remain approximately equivalent, the extent of $S_{B,A}$ conversion is dependent

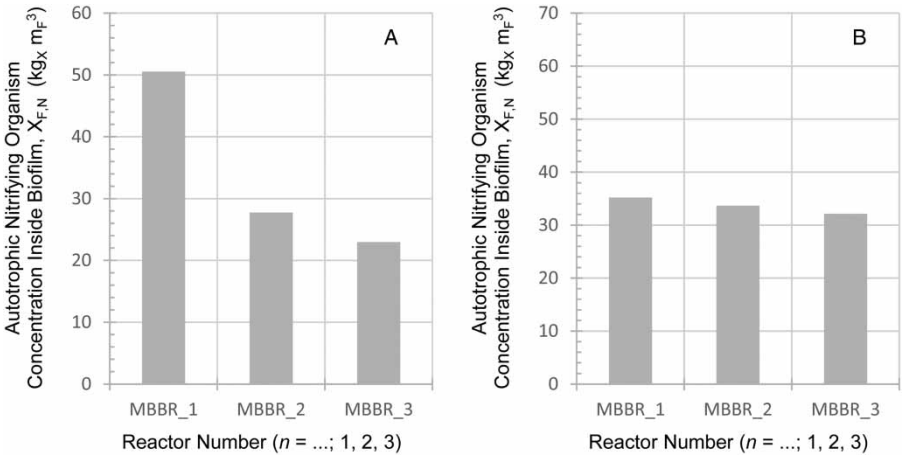

Figure 3 | Comparison of simulated autotrophic nitrifying organism concentrations in the three CFSTRs described as *Configurations A* and *B*.

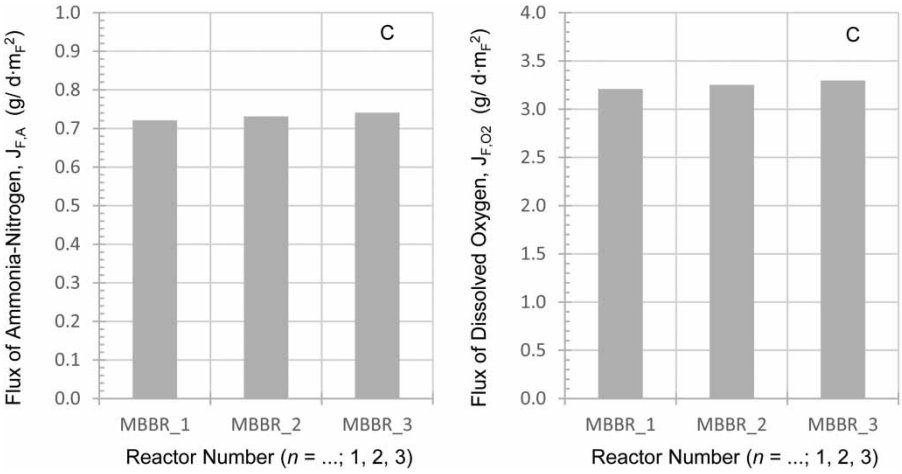

Figure 4 | Comparison of ammonia-nitrogen flux ($J_{F,A}$) and dissolved oxygen flux (J_{F,O_2}) when modeling *Configuration C*.

on $X_{carrier}$ location (i.e., distribution). Figure 5 compares the relative abundance of $X_{F,N}$ in each CFSTR ($X_{F,N}/A_F$) with its percentage of total autotrophic nitrifier abundance in CFSTR n ($X_{F,N,CFSTR\ n}/X_{F,N\text{-}TOTAL}$) in each CFSTR. With $X_{carrier}$ migrating throughout the CFSTRs in series, the value of $X_{F,N}/A_F$ is approximately equivalent. The $X_{F,N}$ abundance increases in each of the three CFSTRs, with the greatest abundance in MBBR_3 resulting from the majority of the A_F being in MBBR_3. Under modeled conditions, $X_{carrier}$ migration results in simulated $J_{F,A}$ and J_{F,O_2} values being approximately equivalent, which – according to Figure 5 – identifies the CFSTR with greatest A_F as having the greatest percentage of total $X_{F,N}$ abundance.

Configuration C was modeled to evaluate the impact that uneven $X_{carrier}$ distribution has on a model-user's ability to describe biofilm reactor performance. This scenario may occur when an elevated approach velocity (e.g., due to a rapid increase in flow rate resulting from peak hydraulic loading conditions or wet-weather) 'pushes' $X_{carrier}$ towards the retention apparatus located at the effluent discharge or point of egress. Mechanically, the model accounts for $X_{carrier}$ migration, but this model does not account for potential diminished oxygen transfer efficiency and the resulting reduction in ammonia-nitrogen uptake (i.e., $J_{F,A}$) when a majority of $X_{carrier}$ has accumulated at the point of egress.

The bulk liquid and its constituents are recycled with $X_{carrier}$ when simulating migration using the method described in this paper. A sufficient recirculation rate through the CFSTR series (which is intended to simulate

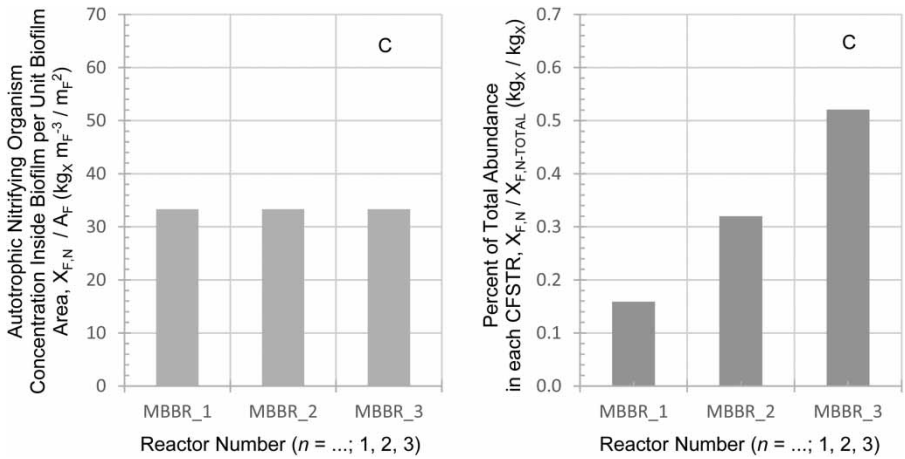

Figure 5 | Autotrophic nitrifier abundance in each CFSTR of *Configuration C*.

plug flow) approaches a completely mixed state. However, a suitable difference exists between liquid, solids, and $X_{carrier}$ residence times that allows a model user to account for a homogeneous $X_{carrier}$ distribution while retaining liquid and solid substrate gradients consistent with those observed in a physical system. Simulations quantify the impact of recirculation on biofilm biomass composition for a recirculation rate of (R=) 2. Reviewing Figure 3(a) indicates 50% change in $X_{F,N}$ between CFSTRs designated MBBR_1 ($n = 1$) and MBBR_3 ($n = 3$) without simulating $X_{carrier}$ migration. Simulation of $X_{carrier}$ migration results (Figure 3(b)) in less than 8% change in $X_{F,N}$ between CFSTRs designated MBBR_1 ($n = 1$) and MBBR_3 ($n = 3$) for a recirculation rate of (R=) 2. Simulation of $X_{carrier}$ migration as *Configuration B* resulted in a 78% $S_{B,A}$ conversion (with a quantifiable reduction in $S_{B,A}$ across each CFSTR in series), which indicates that the series of ($n = 3$) CFSTRs does not have completely mixed contents as a result of the internal recirculation stream flow rate.

Effluent diurnal $S_{B,A}$ profiles from three different simulated systems are shown in Figure 6. Systems with a biofilm compartment were impacted by the diurnal load to a greater extent than the suspended growth systems. This impact is an artefact of the total autotrophic nitrifying

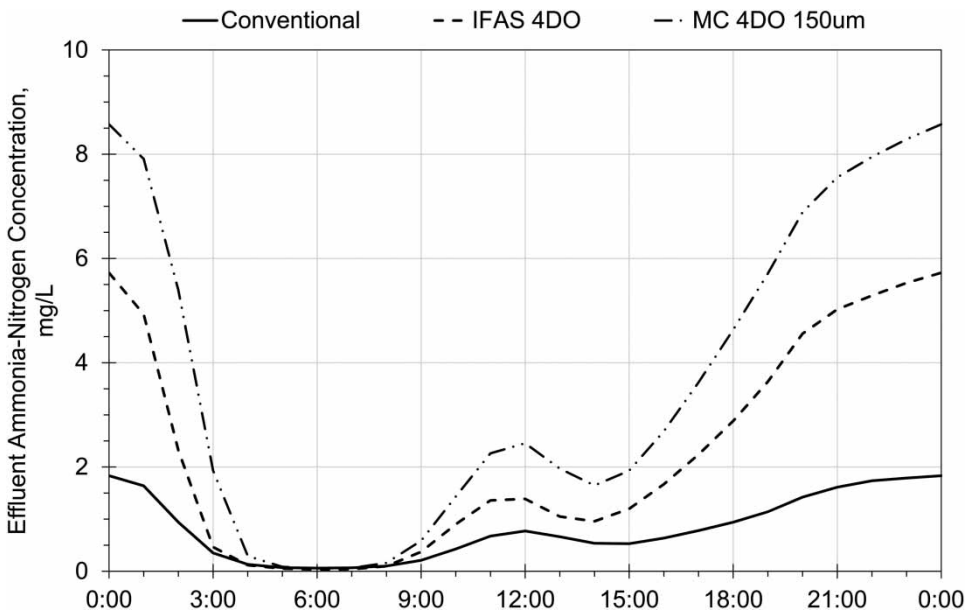

Figure 6 | Diurnal profile of the bulk-liquid ammonia-nitrogen concentration for the suspended growth system ($S_{B,O_2} = 2\,g/m^3$), the IFAS system ($S_{B,O_2} = 4\,g/m^3$), and the migrating $X_{carrier}$ system ($S_{B,O_2} = 4\,g/m^3$, $L_F = 150\,\mu m$).

biomass in the aerobic zones, as shown in Figure 7. The simulated suspended growth process has the highest total mass of autotrophic nitrifiers, followed by the IFAS system, and the migrating $X_{carrier}$ system. The cause of the lower autotrophic nitrifier mass in the migrating $X_{carrier}$ system is a result of the increased competition between bacterial populations within the biofilm compartment. An examination of biofilm biomass in aerobic bioreactor zones of both the IFAS and migrating $X_{carrier}$ systems suggests a lesser autotrophic nitrifier concentration in the migrating $X_{carrier}$ system (autotrophic nitrifier concentration is 20% of the total biomass concentration in migrating $X_{carrier}$ system versus 30–40% in the IFAS system biofilm compartment). This is a result of the biofilm being exposed to readily biodegradable COD driven biochemical transformation processes under anoxic and aerobic conditions, which results in increased competition for space within the biofilm by ordinary heterotrophic organisms. Table 1 summarizes the average daily nutrient discharge concentrations for the systems simulated as *Configuration D*. Table 1 indicates improved nitrate-nitrogen concentration reduction in the migrating $X_{carrier}$ system, which may be a result of its higher ordinary heterotrophic organism concentration.

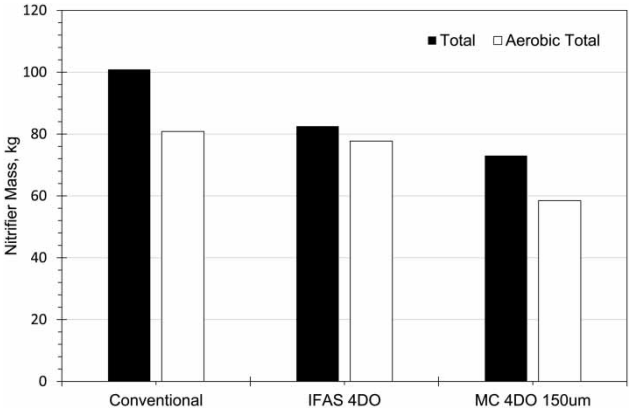

Figure 7 | Comparison of simulated autotrophic nitrifier mass in the entire system (left) with that in the aerobic CFSTRs (right). IFAS – integrated fixed-film activated sludge; DO – dissolved oxygen; MC – mobile [biofilm] carrier.

Table 1 | Average daily effluent nutrient concentrations from simulated *Configuration D*

	Conventional	IFAS	MC
Ammonia, mg NH_4-N/L	0.9	2.6	4.1
Nitrate, mg NO_3-N/L	10.9	14.2	13.3
Phosphate, mg PO_4-P/L	4.6	3.6	4.0

Simulations were executed to evaluate the impact of biofilm thickness (L_F) on the rate of nitrification and the performance of a migrating $X_{carrier}$ system. An examination of Figure 8 shows a negative performance impact as L_F increases from 100 μm to 150 μm and 200 μm. A change in L_F from 100 μm to 150 μm has a minimal impact on

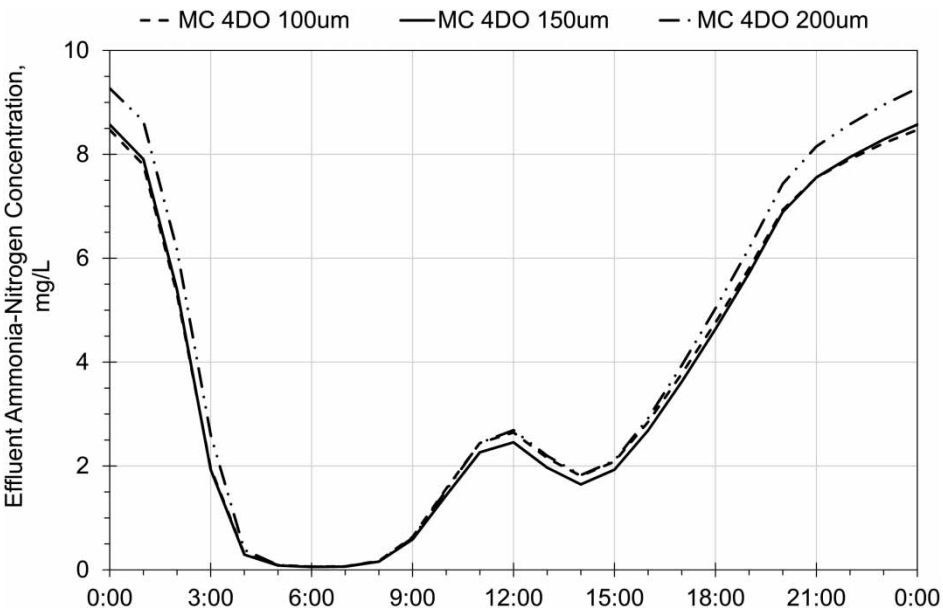

Figure 8 | Impact of biofilm thickness (L_F) on the simulated bulk-liquid ammonia-nitrogen concentration.

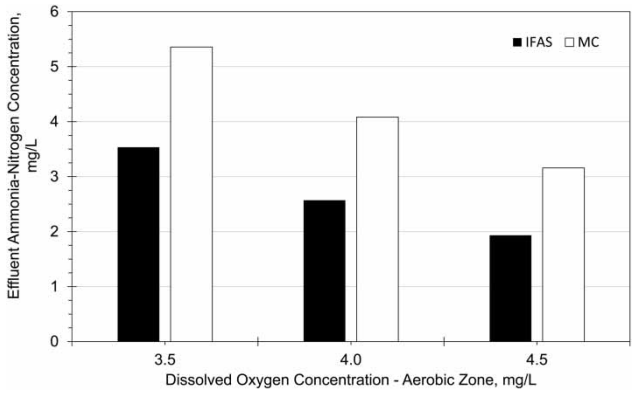

Figure 9 | Impact of bulk-liquid dissolved oxygen concentration on the simulated bulk-liquid ammonia-nitrogen concentration.

system performance, but additional L_F increase to 200 μm results in a marked increase in the effluent ammonia-nitrogen concentration during peak diurnal loading. Simulated mixed-culture biofilms describing simultaneous nitrification and biodegradable COD transformation may accumulate ordinary heterotrophic organisms when arbitrarily increasing L_F and maintaining constant bulk-liquid substrate concentrations. This observation results from the mechanism for simulating biomass decay. Simulated cell lysis – the approach implemented in ASM2d – yields biodegradable COD with increasing ordinary heterotrophic organism concentration. Increased pollutant loading at diurnal peaks results in additional competition for the rate-limiting substrate, namely dissolved oxygen, inside the biofilm. As a result autotrophic nitrifier activity is reduced, and the concentration of ammonia-nitrogen remaining in the simulated bioreactor effluent stream increases. Figure 9 illustrates the impact of varying bulk-liquid dissolved oxygen concentration on the ammonia-nitrogen concentration remaining in the (IFAS and migrating $X_{carrier}$) bioreactor effluent stream. An increased bulk-liquid dissolved oxygen concentration results in a greater driving force that allows the substrate to more deeply penetrate the biofilm, thereby sustaining additional autotrophic nitrifier activity and reducing the ammonia-nitrogen concentration remaining in the simulated bioreactor effluent.

CONCLUSIONS

A biofilm reactor modeling approach accounting for $X_{carrier}$ migration is presented and evaluated. The proposed model is aimed toward overcoming limitations inherent to existing biofilm reactor models. Simulating $X_{carrier}$ migration provides a model user with flexibility to account for the heterogeneity of an $X_{carrier}$ population and associated biofilms throughout a biofilm reactor. The relevance of the proposed biofilm reactor model to engineering situations was evaluated by applying it to scenarios and comparing model results. Simulation of *Configurations A*, *B*, and *C* demonstrates that failure to account for physically present $X_{carrier}$ migration can result in an inaccurate representation of biofilm reactor performance and biofilm biomass distribution. Model results are consistent with the expected influence of $X_{carrier}$ migration, but the model does not account for physical system anomalies such as reduced oxygen transfer efficiency and, therefore, reduced $J_{F,A}$ due to poor air flow and mixing when $X_{carrier}$ concentration exceeds any system-specific acceptable tolerance.

Simulating $X_{carrier}$ migration through anoxic and aerobic zones of an MLE configured bioreactor and a coupled liquid-solids separation unit process showed differences in process performance for IFAS and migrating $X_{carrier}$ systems. The migrating $X_{carrier}$ biofilm system showed less simulated ammonia-nitrogen conversion when compared to an equivalently-sized IFAS process. Model results indicate a decrease in ammonia-nitrogen conversion when the biofilm thickness was arbitrarily increased in a migrating $X_{carrier}$ system. Simulating varying availability of bulk-liquid dissolved oxygen concentration quantified its impact on ammonia-nitrogen removal in systems having a biofilm compartment. Model results suggest that a migrating $X_{carrier}$ system is a viable alternative to IFAS. However, while model results are consistent with the expected influence of $X_{carrier}$ migration, the model does not account for physical system anomalies such as the impact of recirculation pumping on biofilm accumulation/detachment.

ACKNOWLEDGEMENTS

This material was presented during the 5th International Water Association (IWA)/Water Environment Federation (WEF) conference *Wastewater Treatment Modeling 2016* (WWTmod2016), Annecy, France, and was a named component of the session entitled 'Best of WWTmod2016' at the *Water Environment Federation Technical Exhibition and Conference* (WEFTEC), New Orleans, Louisiana, USA (2016).

REFERENCES

Boltz, J. P. & Daigger, G. T. 2010 Uncertainty in bulk-liquid hydrodynamics and biofilm dynamics creates uncertainty in biofilm reactor design. *Water Sci. Technol.* **61** (2), 307.

Boltz, J. P., Johnson, B. R., Daigger, G. T. & Sandino, J. 2009 Modeling integrated fixed-film activated sludge and moving bed biofilm reactor systems I: mathematical treatment and model development. *Water Environ. Res.* **81**, 555–575.

Boltz, J. P., Morgenroth, E. & Sen, D. 2010 Mathematical modelling of biofilms and biofilm reactors for engineering design. *Water Sci. Technol.* **62** (8), 1821–1836.

Boltz, J. P., Morgenroth, E., Brockmann, D., Bott, C., Gellner, W. J. & Vanrolleghem, P. A. 2011 Systematic evaluation of biofilm models for engineering practice: components and critical assumptions. *Water Sci. Technol.* **64** (4), 930–944.

Boltz, J. P., Morgenroth, E., Daigger, G. T., Henze, M., Rittmann, B., Sørensen, K. H., Takács, I., van Loosdrecht, M. C. M., Vanrolleghem, P. & Brockmann, D. 2012 Framework for biofilm model calibration protocol. In: *Proceedings of the 3rd IWA/WEF Wastewater Treatment Modelling Seminar* (WWTmod 2012), Mont-Sainte-Anne, Quebec, Canada.

Brockmann, D., Boltz, J. P., Morgenroth, E., Daigger, G. T., Henze, M., Rittmann, B., Sørensen, K. H., Takács, I., van Loosdrecht, M. C. M. & Vanrolleghem, P. 2013 Applying a framework for calibrating a biofilm reactor model: a full-scale, moving-bed biofilm reactor active in nitrification. In: *Proceedings of the 9th International Conference on Biofilm Reactors*, Paris, France, May 29–31.

Henze, M., Gujer, W., Mino, T. & van Loosdrecht, M. C. M. 2000 *Scientific and Technical Report No. 9: Activated Sludge Models ASM 1, ASM 2, ASM 2d, and ASM 3*. IWA Publishing, London.

Kagawa, Y., Tahata, J., Kishida, N., Matsumoto, S., Picioreanu, C., van Loosdrecht, M. C. M. & Tsuneda, S. 2016 Modeling the nutrient removal process in aerobic granular sludge system by coupling the reactor- and granule-scale models. *Biotechnol. Bioeng.* **112** (1), 53–64.

Kovács, R., Takács, I. & Benke, J. D. 2013 Facilitating biofilm reactor modelling with an easy-to-use spreadsheet-based tool designed for process engineers. In: *IWA Biofilm Conference, 2013*, Paris, France.

McQuarrie, J. P. & Boltz, J. P. 2011 Moving bed biofilm reactor technology: process applications, design, and performance. *Water Environ. Res.* **83** (6), 560–575.

Morgenroth, E., van Loosdrecht, M. C. M. & Wanner, O. 2000 Biofilm models for the practitioner. *Water Sci. Technol.* **41** (4–5), 509–512.

Rittmann, B. E. 1982 Comparative performance of biofilm reactor types. *Biotechnol. Bioeng.* **24**, 1341–1370.

Wanner, O. & Reichert, P. 1996 Mathematical modelling of mixed-culture biofilms. *Biotechnol. Bioeng.* **49** (2), 172–184.

First received 19 December 2016; accepted in revised form 2 March 2017. Available online 17 March 2017